MOLECULAR AND CELLULAR BIOLOGY, Mar. 2005, p. 2320–2330 Vol. 25, No. 6
0270-7306/05/$08.00+0 doi:10.1128/MCB.25.6.2320–2330.2005

Acute Tumor Necrosis Factor Alpha Signaling via NADPH Oxidase in Microvascular Endothelial Cells: Role of $p47^{phox}$ Phosphorylation and Binding to TRAF4

Jian-Mei Li,[1] Lampson M. Fan,[1] Michael R. Christie,[2] and Ajay M. Shah[1]*

Departments of Cardiology[1] and Medicine,[2] Guy's King's and St. Thomas' School of Medicine, King's College London, London, United Kingdom

Received 3 September 2004/Returned for modification 2 October 2004/Accepted 7 December 2004

Tumor necrosis factor alpha (TNF-α) receptor-associated factors (TRAFs) play important roles in TNF-α signaling by interacting with downstream signaling molecules, e.g., mitogen-activated protein kinases (MAPKs). However, TNF-α also signals through reactive oxygen species (ROS)-dependent pathways. The interrelationship between these pathways is unclear; however, a recent study suggested that TRAF4 could bind to the NADPH oxidase subunit $p47^{phox}$. Here, we investigated the potential interaction between $p47^{phox}$ phosphorylation and TRAF4 binding and their relative roles in acute TNF-α signaling. Exposure of human microvascular endothelial cells (HMEC-1) to TNF-α (100 U/ml; 1 to 60 min) induced rapid (within 5 min) $p47^{phox}$ phosphorylation. This was paralleled by a 2.7- ± 0.5-fold increase in $p47^{phox}$-TRAF4 association, membrane translocation of $p47^{phox}$-TRAF4, a 2.3- ± 0.4-fold increase in $p47^{phox}$-$p22^{phox}$ complex formation, and a 3.2- ± 0.2-fold increase in NADPH-dependent O_2^- production (all $P < 0.05$). TRAF4-$p47^{phox}$ binding was accompanied by a progressive increase in extracellular signal-regulated kinases 1 and 2 (ERK1/2) and $p38^{MAPK}$ activation, which was inhibited by an O_2^- scavenger, tiron. TRAF4 predominantly bound the phosphorylated form of $p47^{phox}$, in a protein kinase C-dependent process. Knockdown of TRAF4 expression using siRNA had no effect on $p47^{phox}$ phosphorylation or binding to $p22^{phox}$ but inhibited TNF-α-induced ERK1/2 activation. In coronary microvascular EC from $p47^{phox-/-}$ mice, TNF-α-induced NADPH oxidase activation, ERK1/2 activation, and cell surface intercellular adhesion molecule 1 (ICAM-1) expression were all inhibited. Thus, both $p47^{phox}$ phosphorylation and TRAF4 are required for acute TNF-α signaling. The increased binding between $p47^{phox}$ and TRAF4 that occurs after $p47^{phox}$ phosphorylation could serve to spatially confine ROS generation from NADPH oxidase and subsequent MAPK activation and cell surface ICAM-1 expression in EC.

The cytokine tumor necrosis factor alpha (TNF-α) is capable of activating multiple signal transduction pathways and downstream processes in mammalian cells. In endothelial cells (EC), these processes include the activation of several members of the mitogen-activated protein kinase (MAPK) family, as well as the rapid surface expression of cellular adhesion molecules such as intercellular adhesion molecule 1 (ICAM-1) (6, 17). EC surface expression of ICAM-1 is required for the adhesion of polymorphonuclear neutrophils during vascular inflammation (27).

Occupation of TNF receptors generally leads to the recruitment of diverse intracellular adaptors which then interact with other proteins that form part of downstream signal transduction pathways. With respect to immune and inflammatory responses, the TNF-receptor-associated factors (TRAF1 to TRAF6) are thought to serve as scaffold proteins that directly or indirectly link ligand-occupied receptors of the TNF superfamily to other signaling molecules which subsequently cause the activation of kinases and transcription factors such as the MAPKs and NF-κB, respectively (2, 30). Although many details of the proteins involved in TRAF-induced activation of MAPKs and NF-κB have been elucidated (2, 30), the exact upstream mechanisms through which TRAFs potentiate these pathways remain unclear. In particular, although several proteins capable of direct interactions with TRAFs have been described, the precise functions of most of these proteins in TRAF-mediated signaling are unknown (6).

A separate strand of work has described the involvement of TNF-α-induced generation of intracellular reactive oxygen species (ROS) in downstream signaling, e.g., in EC NF-κB activation and the expression of ICAM-1 (15, 24, 26). TNF-α may stimulate ROS production by several sources, e.g., mitochondria (4), but recent studies have strongly suggested that a major source of ROS is a phagocyte-type NADPH oxidase that is constitutively expressed in EC (3, 9, 13, 22). The EC NADPH oxidase complex contains a catalytic cytochrome b_{558} comprising one $p22^{phox}$ subunit and one Nox subunit and several regulatory subunits, namely $p47^{phox}$, $p40^{phox}$, $p67^{phox}$, and Rac1. The activity of EC NADPH oxidase may be upregulated by mechanical forces, growth factors, angiotensin II, and cytokines such as TNF-α. ROS generated from NADPH oxidase participate in signaling pathways leading to cell proliferation and activation (10, 11, 16, 28). The $p47^{phox}$ regulatory subunit plays a critical role in acute activation of neutrophil NADPH oxidase; phosphorylation of $p47^{phox}$ is thought to relieve inhibitory intracellular interactions and permit the binding of $p47^{phox}$ to $p22^{phox}$, thereby increasing oxidase activation (12).

* Corresponding author. Mailing address: Department of Cardiology, GKT School of Medicine, Bessemer Rd., London SE5 9PJ, United Kingdom. Phone: 44-020-7346 3865. Fax: 44-020-7346 4771. E-mail: ajay.shah@kcl.ac.uk.

The $p47^{phox}$ subunit also appears to be important in EC, and previous studies have shown that TNF-α-induced oxidant generation is abolished in EC from mice lacking $p47^{phox}$ or in wild-type EC transfected in vitro with antisense $p47^{phox}$ cDNA (7, 20).

However, the involvement of ROS generated by NADPH oxidase in TNF-α-induced MAPK activation or ICAM-1 expression remains unclear. Furthermore, it is unclear what the role of ROS-dependent signal transduction as opposed to TRAF-activated pathways is in EC responses to TNF-α. Whereas TRAF-mediated activation of c-Jun N-terminal kinase (JNK) has been quite intensively studied, the involvement of TRAFs in the activation of extracellular signal-regulated kinases 1 and 2 (ERK1/2) or $p38^{MAPK}$ is much less understood (6). Very interestingly, in a recent study a yeast two-hybrid screen found evidence of an association between TRAF4 and $p47^{phox}$ (31), raising the possibility that TRAF-mediated and NADPH oxidase-dependent downstream redox signaling may in fact be linked. However, another recent report indicated that TRAF-mediated signal transduction may involve ROS generation by mitochondria (4). The interrelationship between TNF-α-induced $p47^{phox}$ phosphorylation, $p47^{phox}$-TRAF4 association, and oxidase activation and the contribution of ROS generated by NADPH oxidase to downstream activation of MAPKs (especially ERK1/2 and $p38^{MAPK}$) are therefore of great interest. In the present study, we examined the kinetics of each of these events in response to the acute exposure of human microvascular EC (HMEC-1) to TNF-α. We also more directly investigated the roles of both $p47^{phox}$ and TRAF4 in acute TNF-α-induced MAPK activation and cell surface expression of ICAM-1, using coronary microvascular EC (CMEC) isolated from $p47^{phox-/-}$ mice and siRNA-mediated knockdown of TRAF4, respectively.

MATERIALS AND METHODS

Reagents. 5 (and 6)-Chloromethyl-2′,7′-dichlorodrofluorescein diacetate (DCF) was purchased from Molecular Probes. Affinity-purified rabbit polyclonal antibodies to $p47^{phox}$ and $p22^{phox}$ were a kind gift from F. Wientjes (University College London, London, United Kingdom). The following antibodies were obtained from Santa Cruz Biotechnology: goat polyclonal antibodies to $p22^{phox}$ (C-17), $p47^{phox}$ (C-20), and the corresponding blocking peptides; goat polyclonal antibody specific to the C terminus of TRAF4 (C-20); anti-phospho-JNK (Thr183/Tyr185) and anti-pan-JNK polyclonal antibodies; and anti-phospho-ERK1/2 (Tyr204, E-4) and anti-pan-ERK1/2 monoclonal antibodies. Anti-phospho-$p38^{MAPK}$ (Thr180/Tyr182) and anti-pan-$p38^{MAPK}$ polyclonal antibodies were obtained from Cell Signaling Technology. Anti-α-tubulin and anti-phosphoserine-specific monoclonal antibodies were from Sigma. The siRNA specifically designed to knock down human TRAF4 protein expression and a scrambled negative-control siRNA were purchased from Santa Cruz Biotechnology. [^{32}P]orthophosphate was purchased from Amersham Biosciences, and phosphate-free Dulbecco's modified Eagle's medium (DMEM) was purchased from ICN. Bisindolymaleimide (Bis) was from Calbiochem. All other reagents were obtained from Sigma except where specified.

Cell culture. $p47^{phox}$ null mice ($p47^{phox-/-}$) in a 129sv background were initially generated by and kindly provided by Jurgen Roes (University College London) (14). A colony of these animals is established in our institution (23). All studies conformed to the Guidance on the Operation of Animals (Scientific Procedures) Act, 1986 (Her Majesty's Stationery Office, London, United Kingdom). CMEC were isolated from the hearts of 8- to 10-week-old $p47^{phox-/-}$ and matched wild-type mice as described previously (19). Human dermal microvascular EC (HMEC-1) were obtained from the Centers for Disease Control and Prevention (Atlanta, Ga.) (1). HMEC-1 were cultured in medium 199, and CMEC were cultured in DMEM, both media being supplemented with 10% fetal bovine serum, EC growth supplement (50 μg/ml), epidermal growth factor (10 ng/ml), vascular endothelial growth factor (0.5 ng/ml), ascorbic acid (1 μg/ml), hydrocortisone (1 μg/ml), L-glutamine (2 mmol/liter), penicillin (50 U/ml), and streptomycin (50 μg/ml). CMEC were used at passage 2. For the experiments with TNF-α, adherent cells (90 to 95% confluent) were stimulated with TNF-α (100 U/ml) for 1 to 60 min, washed three times with PBS, detached by scratching, and snap-frozen in liquid nitrogen.

Detection of ROS production. NADPH-dependent O_2^- production by EC homogenate was assessed by lucigenin (5 μmol/liter)-enhanced chemiluminescence as described previously (20, 21). O_2^- production was measured in the absence or presence of NADPH (100 μmol/liter). The specificity of the signal for O_2^- was confirmed by adding either superoxide dismutase (SOD, 200 U/ml) or tiron (5 mmol/liter), a nonenzymatic scavenger of O_2^-, to inhibit the O_2^--dependent chemiluminescence. Each sample was tested in triplicate, and the final data were obtained from at least three separate cell cultures. NADPH-dependent SOD-inhibitable chemiluminescence was determined by subtracting the signal obtained in the combined presence of NADPH and SOD from the signal obtained with NADPH alone. Data are expressed as mean arbitrary light units per minute over a 20-min period.

DCF fluorescence was used as a complementary method for visualization of ROS production. EC were cultured onto chamber slides, washed in Hanks' buffer, and then exposed to TNF-α (100 U/ml) or buffer alone for 30 min. Cells were incubated with 10 μmol of DCF/liter in Hanks' buffer for 30 min at room temperature, and fluorescence was then observed with a Zeiss microscope coupled to a digital imaging system (Improvision) (20). Fluorescence intensity was quantified microscopically from at least three random fields (1,024 by 1,022 pixels; 269.7 by 269.2 μm) per slide (50 cells assessed per slide) and three slides per experimental condition.

In vitro ^{32}P labeling to assess $p47^{phox}$ phosphorylation. HMEC-1 at 90% confluence were labeled with [^{32}P]orthophosphate (100 μCi/ml) at 37°C overnight in phosphate-free DMEM supplemented with 10% fetal calf serum, the latter having been dialyzed against phosphate-free buffer for 24 h before use. After free [^{32}P]orthophosphate was washed off, cells were incubated with or without TNF-α (100 U/ml) in Hanks' balanced salt solution for 15 min. In experiments with the protein kinase C (PKC) inhibitor Bis (10 μmol/liter), Bis was preincubated with the cells for at least 10 min before the addition of TNF-α. Cells were then washed three times with HBSS, detached by scraping into ice-cold mild lysis buffer containing 0.5% NP-40, NaCl (0.15 mol/liter), sodium phosphate (0.01 mol/liter), EDTA (2 mmol/liter), sodium fluoride (50 mmol/liter), sodium vanadate (2 mmol/liter), and aprotinin (100 U/ml) at pH 7.2. Cells were immediately frozen in liquid nitrogen and then lysed by sonication. Whole-cell lysate with a protein concentration of 250 μg per sample was used for immunoprecipitation.

Knockdown of TRAF4 with siRNA. In vitro transfection of HMEC-1 with siRNA was performed according to the manufacturer's (Santa Cruz) protocol with some modifications. Briefly, the day before transfection, HMEC-1 were seeded at 50% confluence in 60-mm-diameter dishes and cultured in growth medium without antibiotics for 24 h. The next day, cells were washed in medium 199, and transfection was performed in 2 ml of serum-free medium 199 without antibiotics. TRAF4-specific or scrambled siRNA was used at a final concentration of 50 nM, and Lipofectamine 2000 (Invitrogen) was used at 1/250 (vol/vol). Four hours after transfection was started, 1 ml of medium 199 with 20% serum was added, and cells were cultured for a further 24 h. After that, the transfection medium was changed to fresh growth medium without antibiotics for another 20 h. Forty-eight hours after transfection, cells were washed, stimulated with or without TNF-α (100 U/ml) for 30 min, detached by scratching, and snap-frozen in liquid nitrogen for subsequent analyses.

Immunoprecipitation and immunoblotting. Immunoprecipitations were performed under nondenaturing conditions using NP-40-lysed and sonicated whole-cell extracts (250 μg of protein) diluted in Tris-HCl (0.05 mol/liter)–NaCl (0.25 mol/liter) buffer (pH 7.4) with protease inhibitors, as described previously (22). $p47^{phox}$ was immunoprecipitated with affinity-purified goat or rabbit polyclonal antibodies coupled to protein G-agarose beads. Immunoblotting of immunoprecipitates was undertaken with affinity-purified rabbit polyclonal antibodies to $p47^{phox}$ and $p22^{phox}$ or with a goat anti-TRAF4 antibody or an anti-phosphoserine-specific monoclonal antibody (1:1,000 dilution). Protein isolated from monocytic U937 cells stimulated with phorbol myristate acetate was used as a positive control for the expression of NADPH oxidase subunits.

In ^{32}P-labeled lysates, an anti-TRAF4 antibody coupled to protein G-agarose beads was first used to immunoprecipitate TRAF4 and any associated proteins (potentially including $p47^{phox}$). To detect phosphorylated $p47^{phox}$ bound to TRAF4, the TRAF4 complexes on agarose beads were spun down and washed three times in mild lysis buffer and $p47^{phox}$ was dissociated from TRAF4 on the agarose beads by adding 1% (wt/vol) sodium deoxycholate and 0.1% sodium dodecyl sulfate in 300 μl of mild lysis buffer warmed to 37°C for 5 min. Any

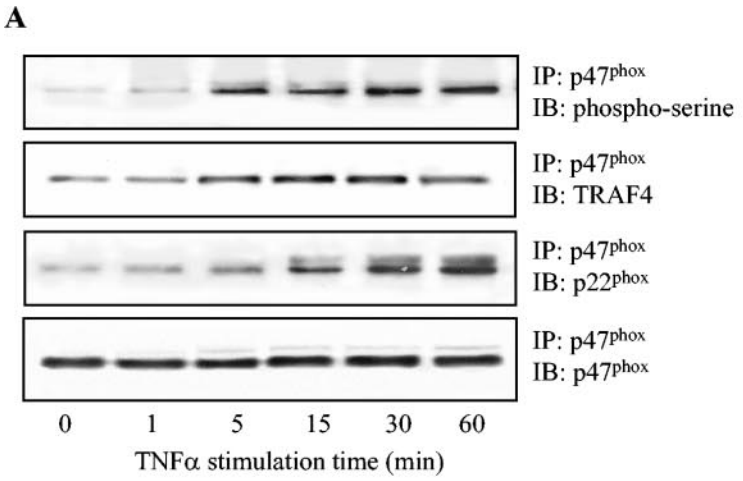

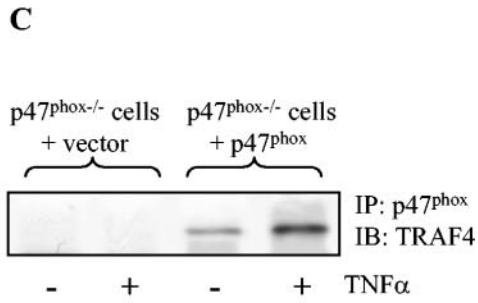

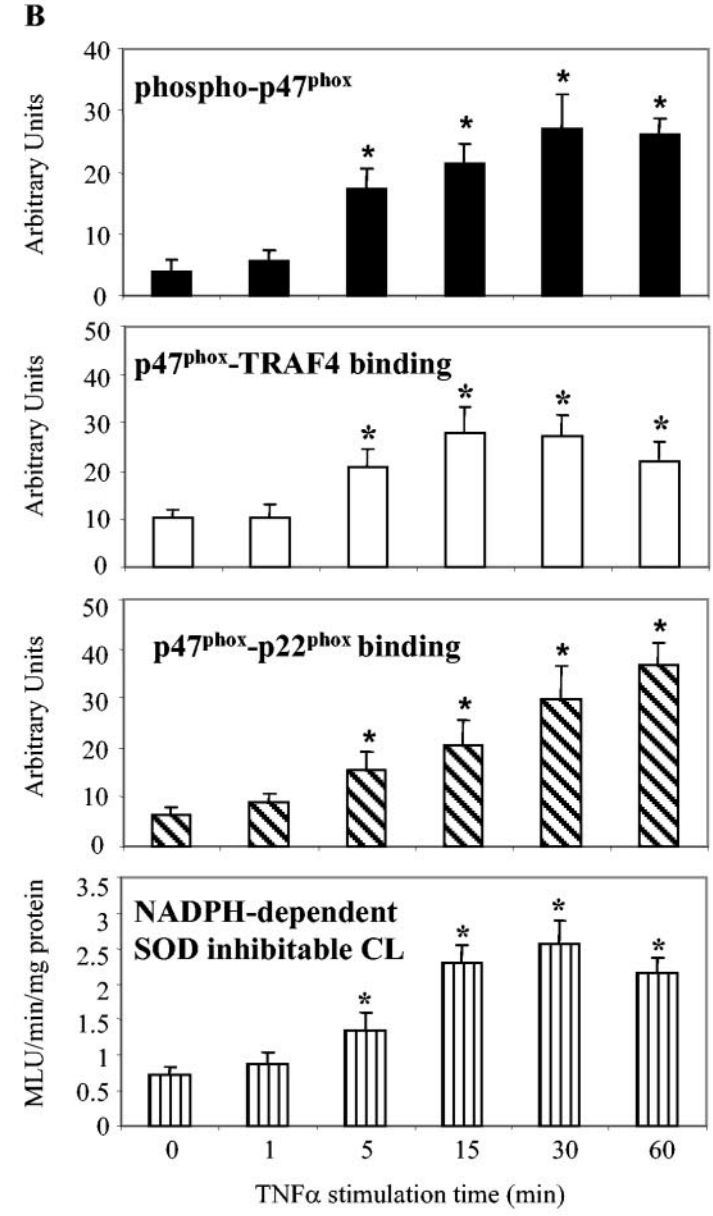

p47^{phox} dissociated was detected by immunoprecipitation using an affinity-purified anti-p47^{phox} antibody. Gels were dried, and phosphorylated p47^{phox} was detected by autoradiography. Proteins in cell lysates and immunoprecipitates were also immunoblotted with antibody to p47^{phox} to assess the amount of total p47^{phox} recovered.

For the detection of MAPK activation, cell homogenates were immunoblotted with specific antibodies against pan- and phospho-ERK1/2, p38^{MAPK}, and JNK. Bands were quantified by densitometry, and values for phospho-MAPK expression were normalized to the amount of total MAPK per sample.

Preparation of membrane and cytoskeletal fractions. In some experiments, we studied the cellular membrane protein fraction, which was prepared as described previously (20). Briefly, cells were detached by scraping and were resuspended in morpholinepropanesulfonic acid (MOPS)-KOH buffer (MOPS-KOH, 20 mmol/liter; sucrose, 250 mmol/liter [pH 7.4]) containing phenylmethylsulfonyl fluoride (1 mmol/liter), EDTA (0.1 mmol/liter), sodium fluoride (50 mmol/liter), sodium vanadate (2 mmol/liter), leupeptin (2 μmol/liter), and pepstatin (2 μmol/liter). Cells were disrupted by quick freezing in liquid nitrogen followed by two cycles (20 s each) of homogenization (Polytron PT 2100) and two cycles of sonication at 100 W for 15 s on ice. The homogenate was quickly centrifuged at 200 × *g* for 5 min to remove any unbroken cells. The membrane-enriched fraction was collected by centrifugation for 60 min at 100,000 × *g*. After another wash, the final pellets were resuspended in sodium dodecyl sulfate buffer and microcentrifuged for 5 min. The protein in the supernatant was used as the membrane fraction.

The extraction of whole-cell protein into Triton X-100-soluble and -insoluble (cytoskeleton) fractions was performed as described previously (20). Briefly, cells were resuspended in ice-cold extraction buffer containing HEPES-Tris (20 mmol of each/liter), NaCl (0.12 mol/liter), KCl (5 mmol/liter), glucose (10 mmol/liter) (pH 7.4), EDTA (0.1 mmol/liter), sodium fluoride (50 mmol/liter), sodium vanadate (2 mmol/liter), leupeptin (2 μmol/liter), pepstatin (2 μmol/liter), and 2% Triton X-100. Cells were disrupted by quick freezing in liquid nitrogen followed by two cycles of sonication at 100 W for 15 s on ice. The whole-cell homogenate was extracted on ice for 20 min. The Triton X-100-soluble and -insoluble fractions were separated by centrifugation at 14,000 × *g* for 15 min. The supernatant (Triton X-100-soluble fraction) was removed, and the pellet (Triton X-100-insoluble cytoskeleton fraction) was washed with Triton buffer to eliminate the residual soluble element. The cytoskeleton fraction was then resuspended in 0.5 ml of Triton buffer, and the soluble protein concentration was determined with a Bio-Rad kit and used for immunoprecipitation or immunoblotting.

Immunofluorescence confocal microscopy. EC were cultured onto four-chamber slides until 80 to 90% confluent. Cells were fixed in acetone-methanol (50% [vol/vol]) and then permeabilized in 0.1% Triton X-100 dissolved in 2% bovine serum albumin-PBS. Slides were blocked with 20% fetal calf serum in PBS for 30 min at room temperature and incubated with primary antibodies diluted (1/50 to 1/250) in 0.1% bovine serum albumin–PBS for 30 min at room temperature (22). Biotin-conjugated anti-rabbit immunoglobulin G (IgG) or anti-mouse IgG (1/500 dilution) was used as the secondary antibody and incubated for 30 min. Specific antibody binding was detected with extravidin labeled with fluorescein isothiocyanate (FITC) (green fluorescence) or tetramethyl rhodamine isothiocyanate (TRITC) (red fluorescence). Normal rabbit or mouse IgG (5 μg/ml) was used instead of primary antibody as the negative control in each case. Confocal microscopy was performed using a Bio-Rad 1024 system. FITC was excited with a 488-nm argon ion laser line, and TRITC was excited with a 543-nm green helium-neon laser line. The emission filters for FITC and TRITC were HQ 515/30 and HQ 580/40, respectively. To avoid bleedthrough, while allowing optimal emission filters to be used, sequential acquisitions were performed (i.e., FITC first followed by TRITC) as described before (22). Images were acquired under identical conditions of exposure time, light intensity, gain, etc.

Statistics. Data are presented as means ± standard deviations of at least three different experiments for each condition. Six mice per group were used for each

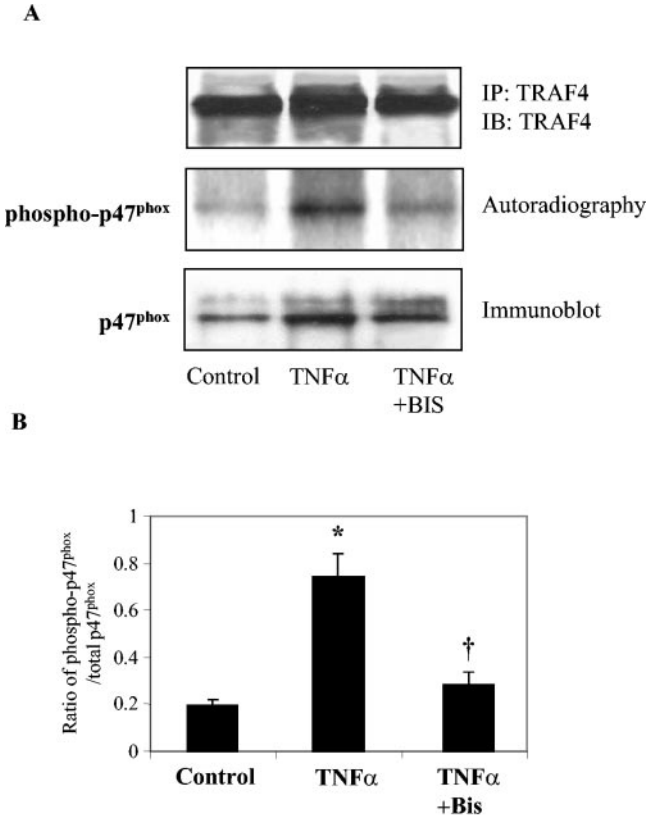

FIG. 2. Assessment of p47^{phox} phosphorylation in p47^{phox}-TRAF4 complexes by sequential immunoprecipitation of ^{32}P-labeled cells. (A) HMEC-1 were labeled with ^{32}P before being treated with TNF-α (100 U/ml, 15 min) in the presence or absence of Bis (10 μmol/liter). Cell lysates were first immunoprecipitated (IP) with an anti-TRAF4 antibody to recover p47^{phox}-TRAF4 complexes, disrupted with detergent, and then reimmunoprecipitated with an anti-p47^{phox} antibody as described in Materials and Methods. IB, immunoblotted. Phosphorylated p47^{phox} was detected by autoradiography (middle panel). The same membrane was immunoblotted with an antibody against p47^{phox} to assess the total amount of p47^{phox} (phosphorylated and nonphosphorylated) bound to TRAF4 (bottom panel). The initial TRAF4 immunoprecipitate was immunoblotted with an anti-TRAF4 antibody (top panel) to confirm equal precipitation of TRAF4. (B) Analysis of relative proportions of phosphorylated p47^{phox} and total p47^{phox}. Autoradiographic and immunoblotted bands were scanned densitometrically, and the backgrounds were subtracted. The ratio of phospho-p47^{phox} to total p47^{phox} was calculated by dividing density results of autoradiography by density results of immunoblotting; the results are expressed as means ± standard deviations for three separate cell cultures and labelings.*, $P < 0.01$ compared to control cells; †, $P < 0.01$ compared to cells stimulated with TNF-α alone.

FIG. 1. Time course of TNF-α-induced p47^{phox} phosphorylation, p47^{phox}-TRAF4 binding, p47^{phox}-p22^{phox} binding, and NADPH-dependent SOD-inhibitable O_2^- production by HMEC-1. (A) Representative immunoblots. p47^{phox} was immunoprecipitated (IP), and then parallel membranes were immunoblotted (IB) either with a phosphoserine-specific antibody (top panel), an anti-TRAF4 antibody (second panel), an anti-p22^{phox} antibody (third panel), or an anti-p47^{phox} antibody (fourth panel). (B) The first three panels show quantitative densitometric analyses of immunoblots. Results are expressed as mean arbitrary absorbance units ± standard deviations obtained from three separate experiments. *, $P < 0.01$ compared to unstimulated cells (i.e., time zero). The bottom panel shows acute TNF-α-induced NADPH-dependent, SOD-inhibitable chemiluminescence (CL) in an HMEC-1 cell homogenate. (C) Control experiment to confirm specific capture of TRAF4 after immunoprecipitation for p47^{phox}. CMEC from p47$^{phox-/-}$ mice (KO cells) were transfected with an empty vector or with p47^{phox} cDNA. Immunoprecipitation was performed for p47^{phox} followed by immunoblotting for TRAF4.

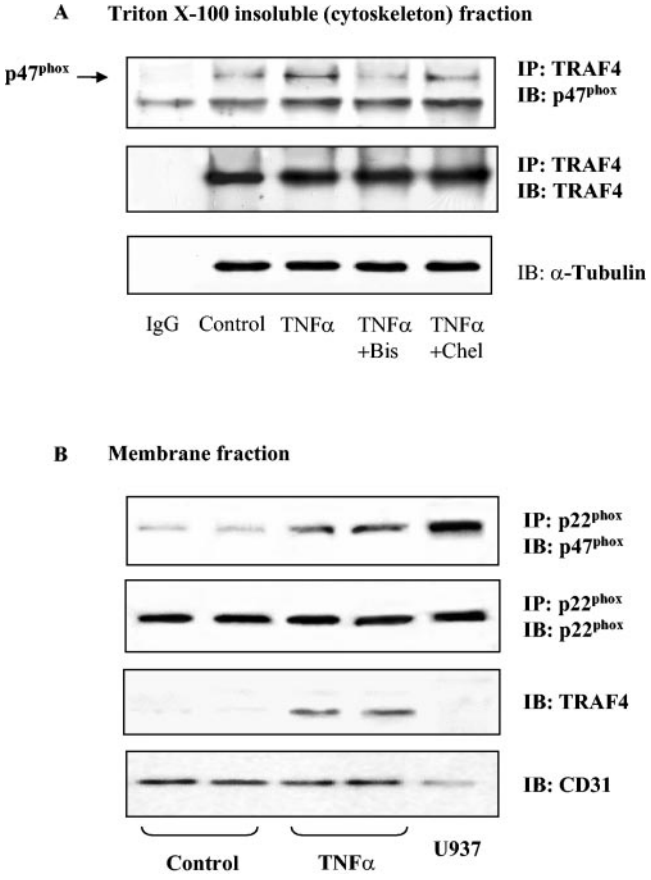

FIG. 3. Effect of TNF-α on association between p47^{phox} and TRAF4 in the cytoskeleton and membrane fractions of HMEC-1. (A) TRAF4 was immunoprecipitated (IP) from the Triton X-100-insoluble (cytoskeleton) fraction, and p47^{phox} was then detected by immunoblotting (IB) in cells stimulated with TNF-α (30 min) either in the presence or absence of the PKC inhibitor Bis or chelerythrine (Chel). Immunoblotting for TRAF4 confirmed equal precipitation. (B) Assessment of translocation and binding to p22^{phox}. p22^{phox} was immunoprecipitated from the cellular membrane fraction, and p47^{phox} was detected by immunoblotting. Protein extracted from U937 cells after stimulation with phorbol myristate acetate was used as a positive control. Similar results were obtained in two independent experiments.

CMEC isolation, and at least three independent isolates were studied. Comparisons were made by one-way analysis of variance or with an unpaired *t* test as appropriate. A *P* value <0.05 was considered statistically significant.

RESULTS

Effect of acute TNF-α stimulation on p47^{phox} phosphorylation, association with TRAF4, and binding to p22^{phox} in HMEC-1. To examine the mechanisms through which p47^{phox} is involved in TNF-α-induced signaling, we first performed immunoprecipitation of p47^{phox} and then studied (i) p47^{phox} phosphorylation, (ii) the binding of p47^{phox} to TRAF4, and (iii) binding of p47^{phox} to a major NADPH oxidase subunit, p22^{phox}, in HMEC-1. In unstimulated cells, a very low level of serine phosphorylation of p47^{phox} was detected with a monoclonal antiphosphoserine-specific antibody (Fig. 1A and B, top panels). TNF-α induced a significant increase in the phospho-p47^{phox} level by 5 min, which peaked at 15 to 30 min and was maintained at 60 min. The same immunoprecipitate was probed on a separate membrane with an anti-TRAF4 antibody (Fig. 1A and B, second panels from the top). In unstimulated cells, there was a readily detectable association of TRAF4 with p47^{phox}. The association between these proteins was significantly increased after 5 min of TNF-α stimulation, peaked at 15 to 30 min (2.7- ± 0.5-fold increase in binding, $P < 0.01$), and then decreased slowly. Note that the total levels of p47^{phox} were similar between groups (Fig. 1A, bottom panel). To confirm that the TRAF4 detected after immunoprecipitation of p47^{phox} represented specific capture, in negative control experiments we demonstrated that no TRAF4 was detectable after immunoprecipitation for p47^{phox} in p47$^{phox-/-}$ cells (Fig. 1C). However, after transfection of these cells with p47^{phox} (20) followed by immunoprecipitation of p47^{phox}, TRAF4 was readily detected by immunoblotting (Fig. 1C).

The membrane used for assessing p47^{phox} serine phosphorylation was reprobed with a p22^{phox} polyclonal antibody to assess the relationship between p47^{phox} phosphorylation and p47^{phox}-p22^{phox} complex formation (Fig. 1A and B, third panels from the top). A low level of p47^{phox}-p22^{phox} protein was readily detectable in the immunoprecipitate of unstimulated EC. Along with p47^{phox} phosphorylation, the amount of p22^{phox} coimmunoprecipitated with p47^{phox} rapidly increased after TNF-α stimulation, being maximal at ~60 min. (2.3- ± 0.4-fold increase, $P < 0.01$). The bottom panel of Fig. 1A shows an immunoblot of total p47^{phox} and confirms equal precipitation of samples.

Aliquots of the protein samples used for detection of p47^{phox} phosphorylation were also examined for NADPH-dependent SOD-inhibitable O_2^- production measured by lucigenin chemiluminescence (Fig. 1B, bottom panel). TNF-α induced a significant increase in NADPH oxidase activity within 5 min, and activity peaked at ~30 min (3.2- ± 0.2-fold increase, $P < 0.05$), broadly in parallel with the time course of the events for which results are shown in the other three panels of Fig. 1B. This level of chemiluminescence is equivalent to approximately 2.5 nmol of O_2^-/min/mg of protein, as assessed by us in previous studies where we conducted a cytochrome *c* reduction assay and a lucigenin assay in parallel under identical conditions (21).

^{32}P labeling to assess the nature of the p47^{phox} species bound to TRAF4. To directly assess whether the p47^{phox} associated with TRAF4 was the phosphorylated species and to estimate the ratio of phosphorylated to total p47^{phox} bound to TRAF4, we performed a sequential immunoprecipitation of TNF-α-stimulated HMEC-1 labeled with ^{32}P, first immunoprecipitating with an anti-TRAF4 antibody and then with an anti-p47^{phox} antibody (see Materials and Methods). The autoradiographs in Fig. 2A (top panel) demonstrate that in unstimulated cells, there was a very low level of phosphorylated p47^{phox} associated with TRAF4. In cells stimulated with TNF-α for 15 min, there was a marked increase in p47^{phox} phosphorylation, which was accompanied by a substantial increase in p47^{phox} association with TRAF4 (Fig. 2A, top and bottom panels). In the presence of the pan-PKC inhibitor Bis, both the amount of p47^{phox} phosphorylation and the total p47^{phox} association with TRAF4 in TNF-α-stimulated cells were significantly decreased. The figure also confirms equal precipitation of TRAF4 in this experiment. Figure 2B shows an analysis of the

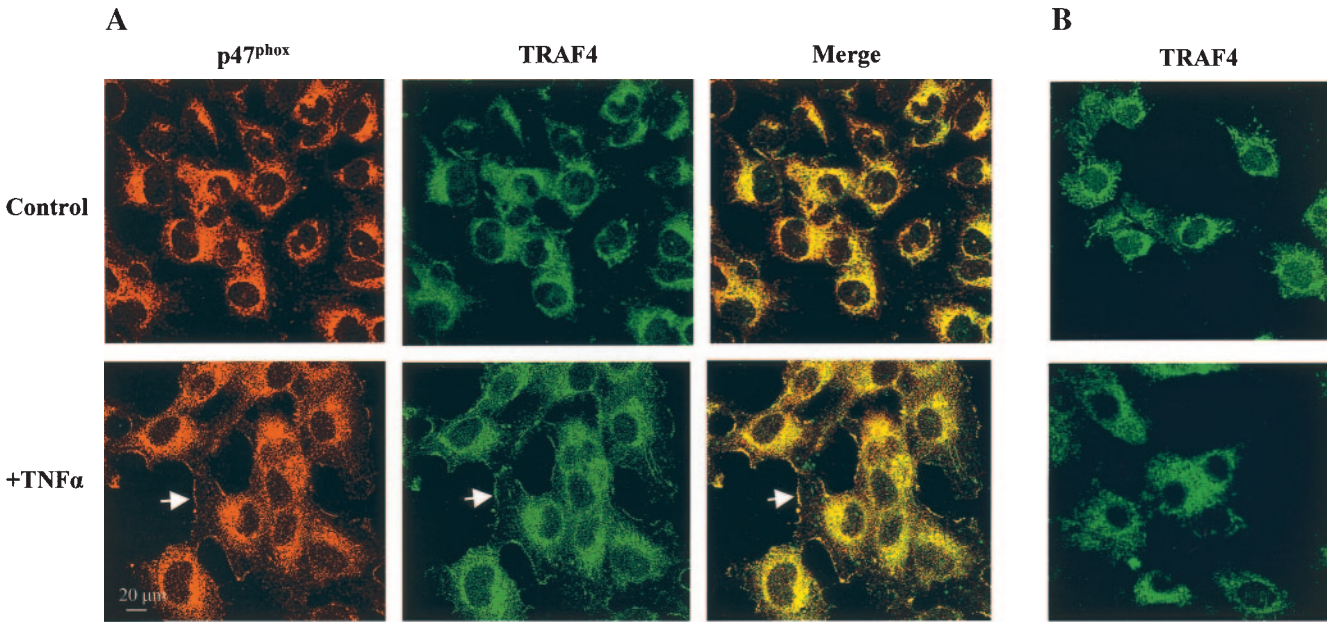

FIG. 4. Immunofluorescence confocal micrographs of HMEC-1 probed for $p47^{phox}$ and TRAF4. (A) HMEC-1 cultured onto chamber slides were exposed to TNF-α or vehicle for 30 min. Slides were double labeled with a rabbit anti-$p47^{phox}$ polyclonal antibody (left panels, red) and a goat anti-TRAF4 polyclonal antibody (middle panels, green). The yellow color in the merged images (right panels) indicates a colocalization of $p47^{phox}$ and TRAF4. The white arrows indicate areas of cell surface membrane labeling. All panels are the same scale. (B) CMEC isolated from $p47^{phox-/-}$ mice and labeled with anti-TRAF4 antibody.

relative proportions of phosphorylated $p47^{phox}$ versus total $p47^{phox}$ in this set of experiments and indicates that after TNF-α stimulation a substantially greater proportion of the $p47^{phox}$ bound to TRAF4 was the phosphorylated form.

TNF-α-induced changes in $p47^{phox}$-TRAF4 association and localization. Since both NADPH oxidase subunits (13, 22) and TRAF4 (31) have been reported to be present preferentially in the detergent-insoluble cytoskeleton fraction, we examined the effect of TNF-α stimulation on the association between $p47^{phox}$ and TRAF4 in the Triton X-100-insoluble (cytoskeleton) fraction. The amount of $p47^{phox}$ associated with TRAF4 was markedly increased in HMEC-1 stimulated with TNF-α (Fig. 3A). However, this increase was substantially inhibited by either of two inhibitors of PKC, namely Bis (10 μmol/liter) or chelerythrine (5 μmol/liter).

In an analogous experiment, the membrane translocation of $p47^{phox}$ and its binding to $p22^{phox}$ were assessed in cell membrane fractions. As shown in Fig. 3B, after immunoprecipitation with an anti-$p22^{phox}$ antibody and immunoblotting for $p47^{phox}$, it was evident that TNF-α stimulation markedly increased the amount of $p47^{phox}$-$p22^{phox}$ complex formation in the membrane fraction. Furthermore, TRAF4 was also detected in the membrane fraction after TNF-α stimulation (Fig. 3B). We were unable to coimmunoprecipitate TRAF4 with $p22^{phox}$ (data not shown). Figure 3B also shows results of immunoblotting for CD31, confirming appropriate separation of membrane fractions.

To assess the effect of TNF-α treatment (30 min) on the interaction between $p47^{phox}$ and TRAF4 and the subcellular distribution of these molecules in HMEC-1 with an alternative method, we used immunofluorescence confocal microscopy (Fig. 4). Cells were double stained by using a rabbit polyclonal antibody to $p47^{phox}$ (red) and a goat polyclonal antibody to TRAF4 (green). In unstimulated cells, both $p47^{phox}$ and TRAF4 had mainly eccentric perinuclear distribution patterns with very little cell surface membrane labeling. Merging of the $p47^{phox}$ and TRAF4 images indicated some colocalization of the two molecules, mainly in the perinuclear region (yellow), but with evidence also of unassociated $p47^{phox}$ and TRAF4. After 30 min of exposure to TNF-α, the intracellular distribution of both $p47^{phox}$ and TRAF4 appeared more organized in reticular patterns extending from the perinuclear region, and there was clear labeling of the cell surface membrane or subsarcolemmal structures, with colocalization of both molecules, as indicated by the yellow color in merged images (Fig. 4, bottom panels, white arrows). In order to confirm the role of $p47^{phox}$ in TNF-α-induced translocation of TRAF4, identical experiments were also performed with CMEC isolated from wild-type and $p47^{phox-/-}$ mice. While treatment of wild-type CMEC with TNF-α resulted in a surface membrane translocation of $p47^{phox}$-TRAF4 similar to that observed in HMEC-1, no translocation of TRAF4 was observed in $p47^{phox-/-}$ CMEC (Fig. 4B).

TNF-α-induced activation of MAPKs in HMEC-1. Next we examined TNF-α-induced MAPK phosphorylation. In unstimulated cells, there was almost no detectable phospho-ERK1/2 in HMEC-1 (Fig. 5). TNF-α caused a rapid phosphorylation of ERK1/2 within 1 min, with phosphorylation peaking at ~30 min and being maintained at the same level at 60 min. The kinetics of TNF-α-induced ERK1/2 activation paralleled the kinetics of TNF-α-induced $p47^{phox}$ phosphorylation and O_2^- production (Fig. 1B).

Similar to ERK1/2, TNF-α induced a significant and rapid increase in $p38^{MAPK}$ phosphorylation within 1 min, with phos-

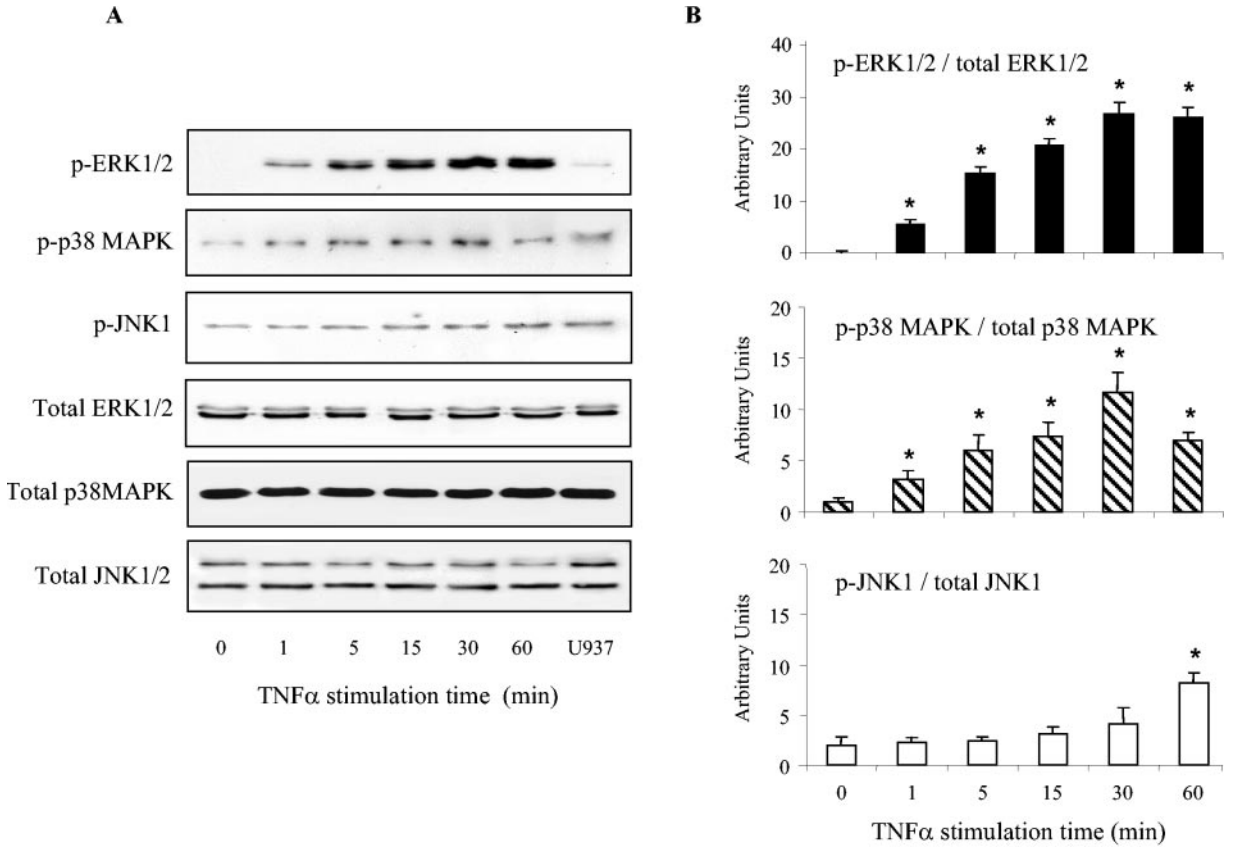

FIG. 5. Time course of TNF-α-induced MAPK activation in HMEC-1. (A) Representative immunoblots showing expression of phospho-ERK1/2, phospho-p38^{MAPK}, and phospho-JNK and corresponding total MAPKs after various periods of exposure to TNF-α. (B) Densitometric quantification of expression level of phospho-ERK1/2, phospho-p38^{MAPK}, and phospho-JNK normalized by respective total ERK1/2, p38^{MAPK}, and JNK expression. Results are means ± standard deviations from three independent experiments. *, $P < 0.01$ for TNF-α-stimulated versus unstimulated (time zero).

phorylation peaking at ~30 min and then decreasing. Interestingly, TNF-α did not induce a significant increase in JNK phosphorylation until 60 min of stimulation (Fig. 3), indicating a divergence between JNK and p38^{MAPK}/ERK1/2 in very early TNF-α signaling.

TNF-α-induced ROS production and MAPK activation in wild-type and p47$^{phox-/-}$ CMEC. In order to directly assess the role of p47^{phox} in TNF-α-induced acute ROS production and MAPK activation, we studied CMEC isolated from wild-type and p47$^{phox-/-}$ mice. DCF fluorescence was used to detect in situ ROS generation. TNF-α (100 U/ml, 30 min) significantly increased DCF fluorescence intensity in wild-type CMEC (52.5 ± 6.2 versus 21.2 ± 4.2 arbitrary units in unstimulated cells; *n*, >300 cells from three independent experiments; $P < 0.01$). However, as expected, no significant increase in DCF fluorescence intensity was found with TNF-α in p47$^{phox-/-}$ CMEC (26.7 ± 3.4 versus 34.2 ± 2.7 arbitrary units in unstimulated cells; $P < 0.01$).

Next we examined MAPK activation in wild-type and p47$^{phox-/-}$ CMEC. In unstimulated cells, there were low levels of phospho-ERK1/2, phospho-p38^{MAPK}, and phospho-JNK detectable (Fig. 6). Exposure of wild-type cells to TNF-α for 30 min significantly increased the levels of phospho-ERK1/2 (2.6- ± 0.5-fold) and phospho-p38^{MAPK} (2.1- ± 0.3-fold) (both $P <$ 0.05), but the level of phospho-JNK was not significantly altered over this time period. In contrast to wild-type CMEC, TNF-α stimulation of p47$^{phox-/-}$ CMEC had no significant effect on the levels of phospho-ERK1/2 or phospho-p38^{MAPK} expression (Fig. 6).

To confirm that the p47^{phox}–dependent effects discussed above were attributable to ROS generation by NADPH oxidase, we examined the effects of a cell-permeable O_2^- scavenger, tiron (5 mmol/liter), or of a flavoprotein inhibitor, diphenyleneiodonium (DPI; 10 μmol/liter), on TNF-α-induced O_2^- production and the activation of ERK1/2, which showed greater changes than the other MAPKs. Wild-type and p47$^{phox-/-}$ CMEC were preincubated with or without tiron or DPI for 30 min and then exposed to TNF-α (100 U/ml) for a further 30 min in the continued presence of inhibitor. Cell homogenates were prepared and examined in parallel for NADPH-dependent O_2^- production by lucigenin chemiluminescence (Fig. 7A) and ERK1/2 phosphorylation by immunoblotting (Fig. 7B and C). Both tiron and DPI abolished the TNF-α-induced increase in NADPH-dependent O_2^- generation by wild-type cells and also abolished the TNF-α-induced increase in ERK1/2 phosphorylation. Interestingly, the levels of O_2^- production and ERK1/2 phosphorylation were reduced by tiron to a level significantly below the basal level in both

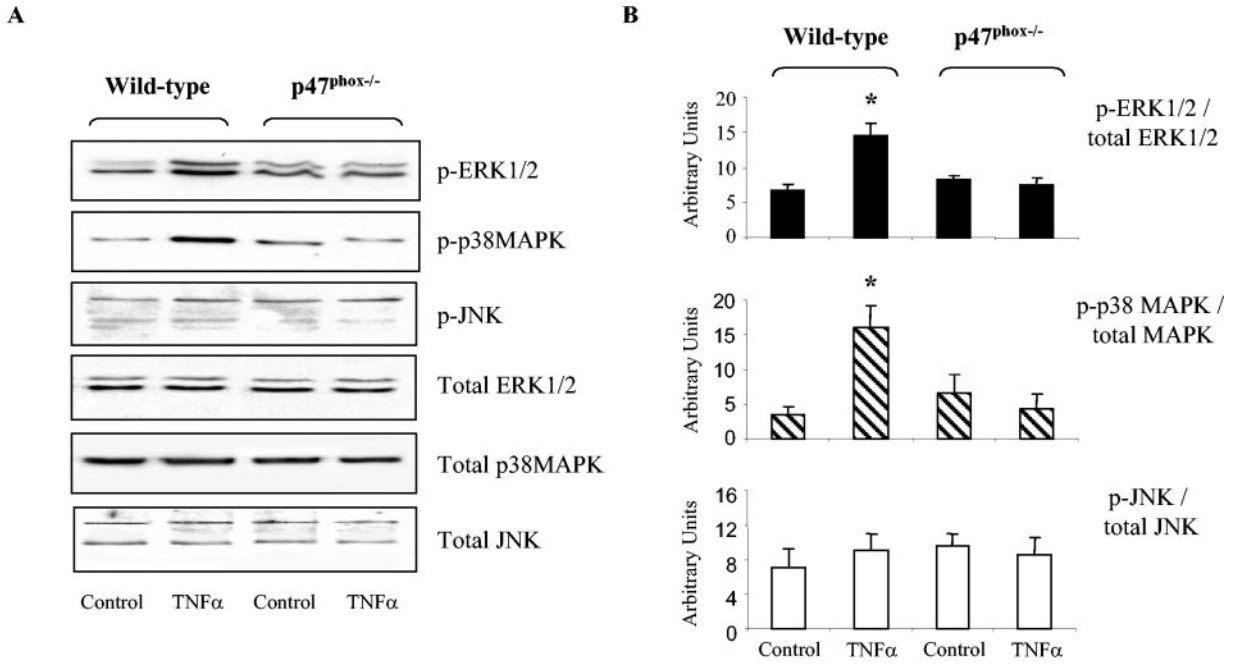

FIG. 6. MAPK activation in wild-type and p47$^{phox-/-}$ CMEC. (A) Representative immunoblots showing expression of phospho-ERK1/2, phospho-p38^{MAPK}, and phospho-JNK and corresponding total MAPKs with or without TNF-α stimulation (30 min). (B) Densitometric quantification of expression levels of phospho-ERK1/2, phospho-p38^{MAPK}, and phospho-JNK normalized by respective total ERK1/2, p38^{MAPK}, and JNK expression. Results are means ± standard deviations from three CMEC isolations (six mice in each group for each isolation) *, $P < 0.01$ comparing TNF-α-stimulated versus unstimulated in each group.

wild-type and p47$^{phox-/-}$ cells. These data confirm a major role of ROS generated from NADPH oxidase in TNF-α-induced ERK1/2 phosphorylation.

Role of TRAF4 in TNF-α-induced ERK activation. To directly assess the role of TRAF4 in TNF-α-induced MAPK activation, further experiments were undertaken in which HMEC-1 were transfected with a specific siRNA to knock down TRAF4 levels. Figure 8A demonstrates that TRAF4 protein expression was substantially reduced after treatment with specific siRNA versus treatment with scrambled control siRNA. In anti-TRAF4 siRNA-treated cells, TNF-α-induced activation of ERK1/2 was abolished. Total levels of ERK1/2 and of p47^{phox} were similar in all groups. HEK293 cells, which are known not to express TRAF4 (6a), showed no activation of ERK1/2 after exposure to TNF-α (Fig. 8A). Knockdown of TRAF4 expression did not inhibit TNF-α-induced phosphorylation of p47^{phox} as assessed by antiphosphoserine antibodies (Fig. 8B, top panel), nor did it affect complex formation between p47^{phox} and p22^{phox} (Fig. 8B, bottom panel). These data clearly indicate that not only p47^{phox} but also TRAF4 is required for the acute activation of ERK1/2 by TNF-α.

Role of p47^{phox} and O_2^- in TNF-α-induced acute cell surface expression of ICAM-1. Finally, we investigated the requirement of p47^{phox} for TNF-α-induced cell surface expression of ICAM-1 in studies with wild-type and p47$^{phox-/-}$ CMEC. In wild-type CMEC, stimulation with TNF-α (100 U/ml, 60 min) caused a distinct cell surface expression of ICAM-1, as assessed by immunofluorescence confocal microscopy (Fig. 9, top panels). This effect was inhibited by tiron (5 mmol/liter), confirming the role of O_2^- in this process. In contrast, TNF-α stimulation failed to induce surface expression of ICAM-1 in p47$^{phox-/-}$ CMEC (Fig. 9, bottom panels). Normal rabbit IgG (5 μg/ml) was used as a negative control (Fig. 9, bottom right panel).

DISCUSSION

On the basis of previous studies, it is known that TRAF-mediated signal transduction is important in TNF-α-induced activation of MAPKs, in particular JNK (2, 6, 30). It has also been reported that TNF-α-induced ROS generation is involved in EC responses such as the activation of NF-κB and expression of ICAM-1 (15, 24, 26) and that these ROS may derive from NADPH oxidase (7, 20) or other sources (4). However, the relative roles of NADPH oxidase activation and TRAF-mediated signaling in acute EC responses to TNF-α and the interrelationship between these, if any, have been unclear. The present study addressed this question in EC, focusing particularly on TNF-α-induced MAPK activation. We show that the acute response to TNF-α involves a rapid PKC-dependent phosphorylation of p47^{phox}, an increase in p47^{phox}-TRAF4 association, translocation of p47^{phox}-TRAF4 to the cell membrane, increased formation of p47^{phox}-p22^{phox} complexes, and activation of NADPH oxidase and ROS generation. NADPH oxidase activation leads to a rapid (within 5 min) activation of ERK1/2 and p38^{MAPK} (but not JNK), which requires both p47^{phox} and TRAF4 since it is inhibited either in the absence of p47^{phox} or after knockdown of TRAF4. These results therefore suggest a central role for p47^{phox}-TRAF4 interaction and NADPH oxidase activation in TNF-α-induced

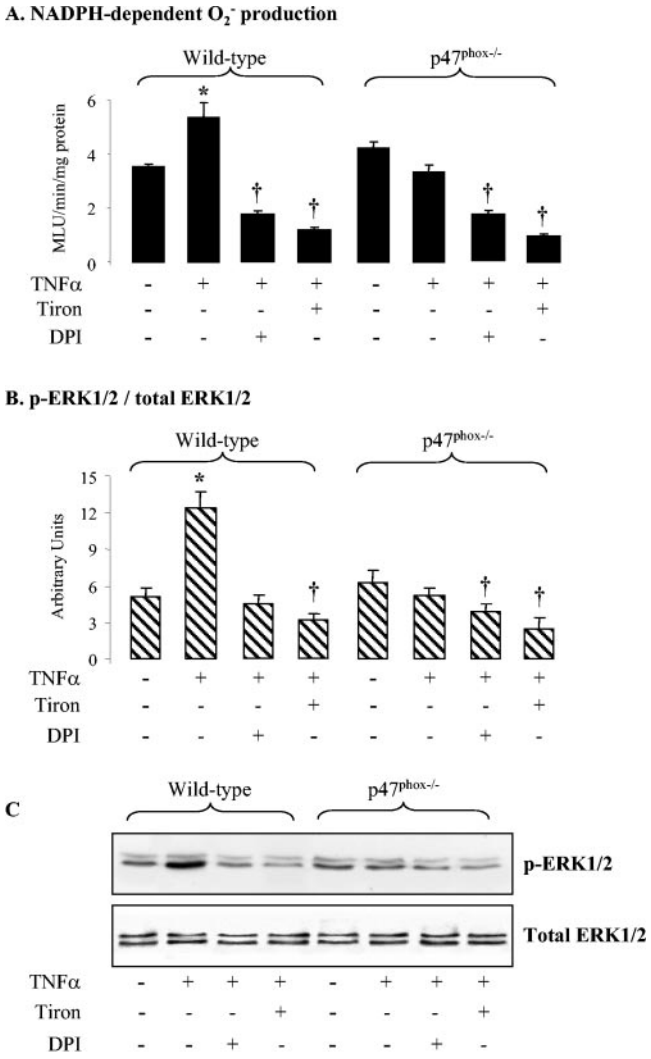

FIG. 7. Effects of tiron and DPI on TNF-α-induced ERK1/2 activation in wild-type and $p47^{phox-/-}$ CMEC. (A) NADPH-dependent O_2^- production by wild-type and $p47^{phox-/-}$ CMEC homogenates measured by lucigenin chemiluminescence. Results are expressed as mean light units (MLU) per minute per milligram of protein. (B) Densitometric quantification of expression levels of phospho-ERK1/2 normalized by total ERK1/2 in wild-type and $p47^{phox-/-}$ CMEC. Results are means ± standard deviations from three CMEC isolations (six mice from each group for each isolation). *, significantly higher ($P < 0.01$) value than control unstimulated value; †, significantly lower ($P < 0.01$) value than control unstimulated value. (C) Representative immunoblot showing ERK1/2 phosphorylation in wild-type and $p47^{phox-/-}$ CMEC stimulated with TNF-α or unstimulated in the presence or absence of tiron or DPI.

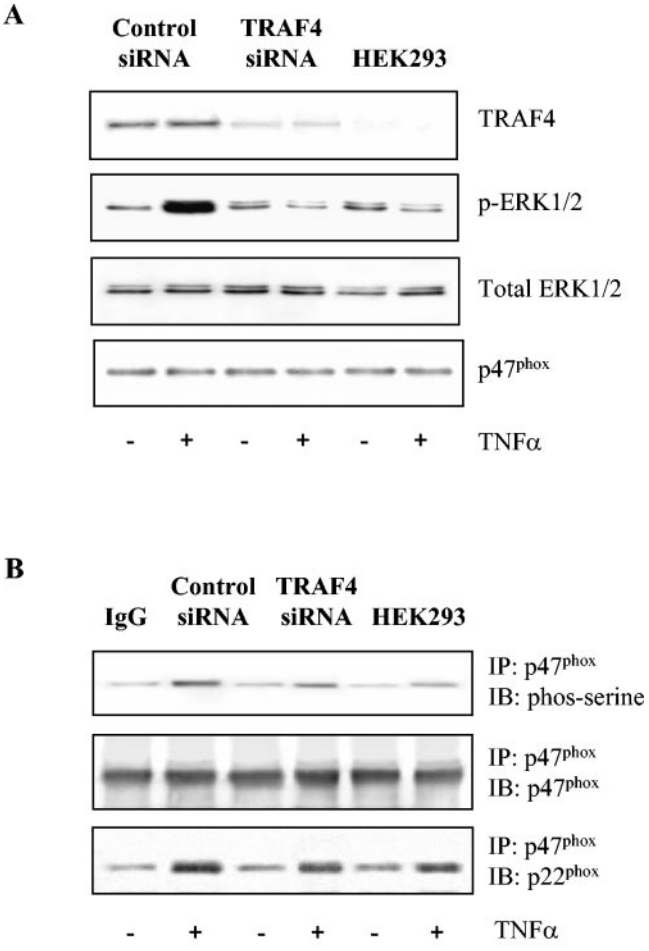

FIG. 8. Effect of siRNA-mediated knockdown of TRAF4 on acute TNFα-induced ERK1/2 activation and $p47^{phox}$ phosphorylation in HMEC-1. (A) Immunoblotting for TRAF4 expression and ERK1/2 activation after anti-TRAF4 siRNA treatment. HEK293 cells, which do not express TRAF4 endogenously (6a), were used as a negative control for TRAF4 expression. (B) Assessment of serine phosphorylation of $p47^{phox}$ after knockdown of TRAF4. The same blot was reprobed with an anti-$p47^{phox}$ antibody, while a parallel membrane was immunoblotted (IB) for $p22^{phox}$. IP, immunoprecipitated.

EC activation of ERK1/2 and $p38^{MAPK}$. We also find that the $p47^{phox}$ that associates with TRAF4 upon stimulation with TNF-α is predominantly the phosphorylated species and that $p47^{phox}$-TRAF4 interaction is PKC dependent, suggesting that phosphorylation of $p47^{phox}$ may be an important event in formation of the $p47^{phox}$-TRAF4 complexes.

TNF-α signaling is initiated by its binding to TNF-α receptors, which leads to the recruitment of several adaptor proteins (2, 6). Recently, the TRAFs have been recognized to serve as scaffold proteins that link the TNF receptors to signaling cascades, including activation of MAPKs and NF-κB (6, 30). TRAF4 is predominately intracellularly located but can be directed to the cell surface receptor sites where it binds through its C-TRAF domain (8). In a recent study where TRAF4 and $p47^{phox}$ were transfected into Phoenix-293 cells, they were found primarily in the detergent-insoluble cytoskeleton fraction of these cells and could bind to each other through their C termini (31). In the present study, the use of multiple complementary approaches (including coimmunoprecipitation, autoradiography, assessment of cellular fractions, and confocal microscopy) indicated that a small amount of $p47^{phox}$ was associated with TRAF4 in unstimulated HMEC-1, mainly in the perinuclear region in a cytoskeletal fraction. Upon stimulation with TNF-α, however, there was a marked increase in association between phosphorylated $p47^{phox}$ and TRAF4, which was accompanied by translocation of the $p47^{phox}$-TRAF4 complex to the membrane fraction. Confocal

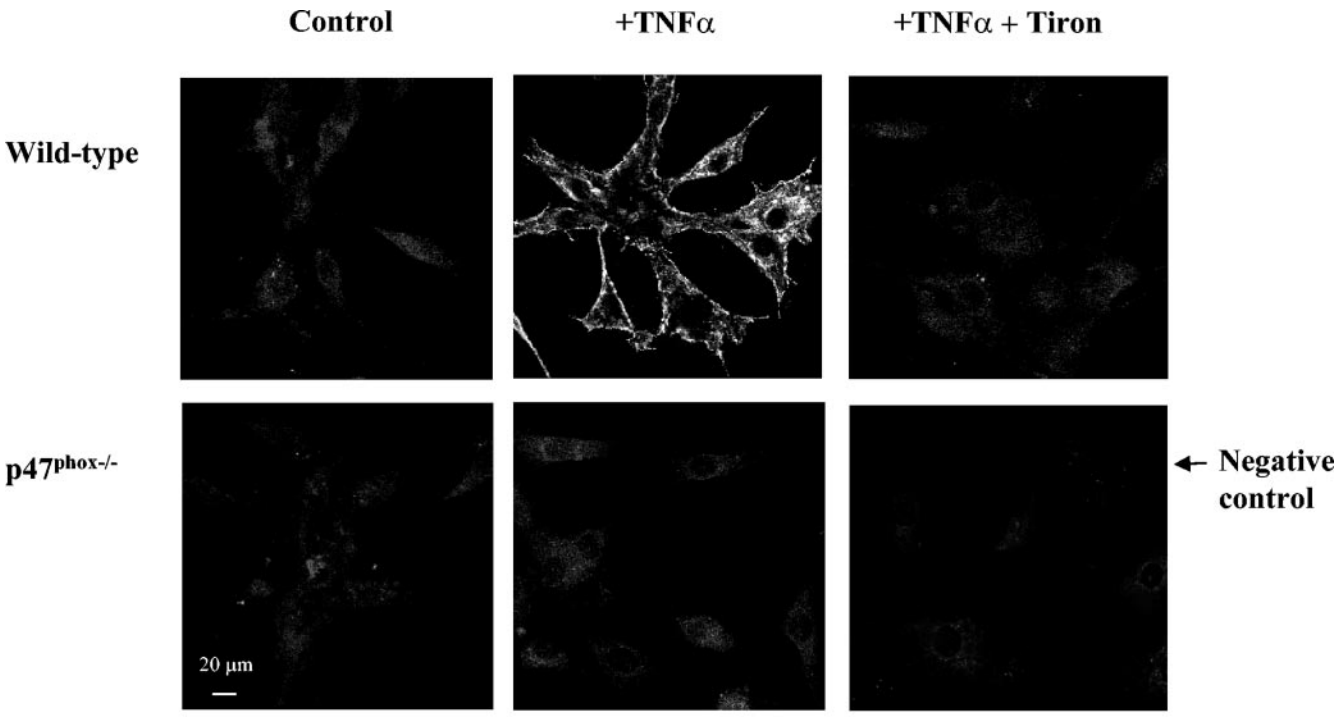

FIG. 9. Immunofluorescence confocal micrographs of wild-type and $p47^{phox-/-}$ CMEC showing surface expression of ICAM-1. Nonpermeabilized CMEC cultured onto chamber slides were stimulated with TNF-α (100 U/ml, 60 min) or not stimulated in the presence or absence of tiron. Cells were then probed for the surface membrane expression of ICAM-1. Normal rabbit IgG (5 μg/ml) was used as a negative control (lower right panel). All panels are the same scale.

microscopy indicated that at least a component of the $p47^{phox}$-TRAF4 complexes was translocated to the cell surface membrane (or subsarcolemmal structures). The kinetics of $p47^{phox}$ phosphorylation closely paralleled those of $p47^{phox}$-TRAF4 and $p47^{phox}$-$p22^{phox}$ complex formation and NADPH oxidase activation, whereas inhibition of $p47^{phox}$ phosphorylation by inhibitors of PKC inhibited $p47^{phox}$-TRAF4 binding and membrane translocation of complexes.

The binding of $p47^{phox}$ to TRAF4 is reported to involve residues 299 to 390 in the C terminus of $p47^{phox}$ (31), which also contain a cluster of serine residues that form potential PKC phosphorylation sites (29). Serine phosphorylation of $p47^{phox}$ in this region is thought to induce conformational changes in $p47^{phox}$ needed for NADPH oxidase activation (18). It is possible that $p47^{phox}$ phosphorylation also facilitates its interaction with TRAF4. In this regard, it is of interest that TNF-α-induced NADPH oxidase activation is reported to involve PKCζ (7), and atypical PKC isoforms as well as cellular structural proteins have been reported to be potential binding partners for TRAF (30). The findings in the current study that both $p47^{phox}$ and TRAF4 are required for TNF-α-induced ERK1/2 activation and that $p47^{phox}$-TRAF4 binding appears central to this activation suggest that a $p47^{phox}$-TRAF4 complex could serve to localize redox-regulated signaling molecules downstream of TRAF4 into close proximity to active NADPH oxidase. In such a scheme, the level of $p47^{phox}$ phosphorylation and its binding to TRAF4 may regulate not only the local level of intracellular ROS (by activating NADPH oxidase) but also the spatial confinement of ROS close to appropriate downstream target proteins, e.g., ERK1/2 and $p38^{MAPK}$. Consistent with such a scheme, while knockdown of TRAF4 did not interfere with $p47^{phox}$ phosphorylation (or $p47^{phox}$-$p22^{phox}$ complex formation), it inhibited ERK1/2 activation. Indeed, there was a close relationship between the kinetics of TNF-α-induced $p47^{phox}$ phosphorylation, $p47^{phox}$-TRAF4 complex formation, NADPH oxidase activation, and the phosphorylation of ERK1/2 and $p38^{MAPK}$. Interestingly, the levels of phospho-JNK (which may also be activated by TNF-α in a redox-sensitive manner [31]) were not significantly increased in the first 30 min or so after exposure to TNF-α at a time when ERK1/2 and $p38^{MAPK}$ were significantly phosphorylated, indicating a divergent activation of these pathways and suggesting that JNK activation may be more involved in later TNF-α-induced events.

The critical roles of $p47^{phox}$ and NADPH oxidase in mediating acute TNF-α signaling were directly demonstrated by using CMEC from $p47^{phox-/-}$ mice in which TNF-α-induced ROS production and ERK1/2 and $p38^{MAPK}$ phosphorylation were abolished. Furthermore, the inhibition of ERK1/2 phosphorylation either by tiron, an O_2^- scavenger, or by DPI, a flavoprotein inhibitor, provided corroborative evidence that the $p47^{phox}$- and NADPH oxidase-dependent effects were indeed attributable to O_2^-. These findings also clearly indicate that TNF-α-induced ERK1/2 activation involves O_2^- rather than some other TRAF-mediated signal.

During inflammation, a rapid increase in the surface expression of EC adhesion molecules is a prerequisite for the early transmigration of polymorphonuclear cells through the vessel wall (25). TNF-α dramatically induces adhesion molecule surface expression and EC adhesivity within minutes of challenge

(17). Very recently, the importance of NADPH oxidase in the regulation of TNF-α-induced EC adhesion molecule expression has been suggested by the finding that dominant negative Rac1 (which may disrupt NADPH oxidase activity) inhibits TNF-α-induced expression of ICAM-1, vascular cell adhesion molecule 1, and E selectin in human aortic EC (5). Among the adhesion molecules, ICAM-1 serves as a counterreceptor for leukocyte b2-CD11/CD18 integrins and plays an important role in the firm adhesion and the stable arrest of polymorphonuclear cells onto EC. In the present study, we focused on very early (within an hour) TNF-α-induced surface expression of ICAM-1. We found that acute TNF-α-induced early EC surface ICAM-1 expression is $p47^{phox}$ dependent and requires an intracellular burst of O_2^-. As shown by confocal microscopy, acute exposure to TNF-α caused cell surface ICAM-1 expression in wild-type CMEC, which was completely blocked by preincubation of cells with tiron; the effect was also absent in $p47^{phox-/-}$ CMEC.

In summary, we present evidence in the current report for a TNF-α-activated redox signaling cascade in microvascular EC which involves PKC-dependent phosphorylation of $p47^{phox}$, $p47^{phox}$-TRAF4 binding and translocation, NADPH oxidase activation, and the specific activation of $ERK1/2$ and $p38^{MAPK}$ together with early-onset cell surface expression of ICAM-1. The level of $p47^{phox}$ phosphorylation and the binding of phosphorylated $p47^{phox}$ to TRAF4 may be critical factors in regulating acute TNF-α signaling, with TRAF4 serving as a link between $p47^{phox}$/NADPH oxidase on the one hand and specific redox-sensitive targets such as ERK1/2 or upstream MAPK-activating proteins on the other. These results provide an insight into the potential mechanisms through which NADPH oxidase-derived ROS may result in spatially confined or selective TNF-α-induced redox signaling in EC.

ACKNOWLEDGMENTS

This work was supported by British Heart Foundation (BHF) Program Grant RG/98008 and BHF project grant PG/02/112. L.M.F. was funded by a Wellcome Trust Vacation Scholarship. A.M.S. holds the BHF Chair of Cardiology in King's College London.

REFERENCES

1. **Ades, E. W., F. J. Candal, R. A. G. V. G. Swerlick, S. Summers, D. C. Bosse, and T. J. Lawley.** 1992. HMEC-1: establishment of an immortalized human microvascular endothelial cell line. J. Investig. Dermatol. **99:**683–690.
2. **Aggarwal, B. B.** 2003. Signalling pathways of the TNF superfamily: a double-edged sword. Nat. Rev. Immunol. **3:**745–756.
3. **Bayraktutan, U., L. Blayney, and A. M. Shah.** 2000. Molecular characterization and localization of the NAD(P)H oxidase components gp91-phox and p22-phox in endothelial cells. Arterioscler. Thromb. Vasc. Biol. **20:**1903–1911.
4. **Chandel, N. S., P. T. Schumacker, and R. H. Arch.** 2001. Reactive oxygen species are downstream products of TRAF-mediated signaling transduction. J. Biol. Chem. **276:**42728–42736.
5. **Chen, X.-L., Q. Zhang, R. Zhao, X. Ding, P. E. Tummala, and R. M. Medford.** 2003. Rac1 and superoxide are required for the expression of cell adhesion molecules induced by tumor necrosis factor-α in endothelial cells. J. Pharmacol. Exp. Ther. **305:**573–580.
6. **Dempsey, P. W., S. E. Doyle, J. Q. He, and G. Cheng.** 2003. The signaling adaptors and pathways activated by TNF superfamily. Cytokine Growth Factor Rev. **14:**193–209.

6a. **Fleckenstein, D. S., W. G. Dirks, H.G. Drexler, and H. Quentmeier.** 2003. Tumor necrosis factor receptor-associated factor 4 (TRAF4) is a new binding partner for the p70S6 serine/threonine kinase. Leuk. Res. **27:**687–694.

7. **Frey, R. S., A. Rahman, J. C. Kefer, R. D. Minshall, and A. B. Malik.** 2002. PKCζ regulates TNF-α-induced activation of NADPH oxidase in endothlial cells. Circ. Res. **90:**1012–1019.
8. **Glauner, H., D. Siegmund, H. Motejadded, P. Scheurich, F. Henkler, O. Janssen, and H. Wajant.** 2002. Intracellular localization and transcriptional regulation of tumor necrosis factor (TNF) receptor-associated factor 4 (TRAF4). Eur. J. Biochem. **269:**4819–4829.
9. **Görlach, A., R. P. Brandes, K. Nguyen, M. Amidi, F. Dehghani, and R. Busse.** 2000. A gp91phox containing NADPH oxidase selectively expressed in endothelial cells is a major source of oxygen radical generation in the arterial wall. Circ. Res. **87:**26–32.
10. **Görlach, A., T. Kietzmann, and J. Hess.** 2002. Redox signaling through NADPH oxidases: involvement in vascular proliferation and coagulation. Ann. N.Y. Acad. Sci. **973:**505–507.
11. **Griendling, K. K., D. Sorescu, and M. Ushio-Fukai.** 2000. NAD(P)H oxidase: role in cardiovascular biology and disease. Circ. Res. **86:**494–501.
12. **Groemping, Y., K. Lapouge, S. Smerdon, and K. Rittinger.** 2003. Molecular basis of phosphorylation-induced activation of the NADPH oxidase. Cell **113:**343–355.
13. **Gu, Y., Y. C. Xu, R. F. Wu, R. F. Souza, F. E. Nwariaku, and L. S. Terada.** 2002. TNFα activates c-Jun amino terminal kinase through $p47^{phox}$. Exp. Cell Res. **272:**62–74.
14. **Harbord, M., M. Novelli, B. Canas, D. Power, C. Davis, J. Godovac-Zimmermann, J. Rose, and A. W. Segal.** 2002. Ym1 is a neutrophil granule protein that crystalizes in $p47^{phox}$-deficient mice. J. Biol. Chem. **277:**5468–5475.
15. **Hashimoto, S., Y. Gon, K. Matsumoto, I. Takeshita, and T. Horie.** 2001. N-acetylcysteine attenuates TNF-α-induced p38 MAP kinase activation and p38 MAP kinase-mediated IL-8 production by human pulmonary vascular endothelial cells. Br. J. Pharmacol. **132:**270–276.
16. **Irani, K.** 2000. Oxidant signaling in vascular cell growth, death, and survival: a review of the roles of reactive oxygen species in smooth muscle and endothelial cell mitogenic and apoptotic signaling. Circ. Res. **87:**179–183.
17. **Javaid, K., A. Rahman, K. N. Anwar, R. S. Frey, R. D. Minshall, and A. B. Malik.** 2003. Tumor necrosis factor-α induces early-onset endothelial adhesivity by protein kinase Cζ-dependent activation of intercellular adhesion molecule-1. Circ. Res. **92:**1089–1097.
18. **Lee, J. H., K. S. Lee, T. Chung, and J.-W. Park.** 2000. C-terminal region of the cytosolic subunit $p47^{phox}$ is a primary target of conformational change during the activation of leukocyte NADPH oxidase. Biochimie **82:**727–732.
19. **Li, J.-M., A. M. Mullen, and A. M. Shah.** 2001. Phenotypic properties and characteristics of superoxide production by mouse coronary microvascular endothelial cells. J. Mol. Cell. Cardiol. **33:**1119–1131.
20. **Li, J.-M., A. M. Mullen, S. Yun, F. Wientjes, G. Y. Brouns, A. J. Thrasher, and A. M. Shah.** 2002. Essential role of the NADPH oxidase subunit $p47^{phox}$ in endothelial cell superoxide production in response to phorbol ester and tumor necrosis factor-α. Circ. Res. **90:**143–150.
21. **Li, J.-M., and A. M. Shah.** 2001. Differential NADPH- versus NADH-dependent superoxide production by phagocyte-type endothelial cell NADPH oxidase. Cardiovasc. Res. **52:**477–486.
22. **Li, J.-M., and A. M. Shah.** 2002. Intracellular localization and pre-assembly of the NADPH oxidase complex in cultured endothelial cells. J. Biol. Chem. **277:**19952–19960.
23. **Li, J.-M., and A. M. Shah.** 2003. Mechanism of endothelial cell NADPH oxidase activation by angiotensin II: role of the $p47^{phox}$ subunit. J. Biol. Chem. **278:**12094–12100.
24. **Marui, N., M. K. Offermann, R. Swerlick, C. Kunsch, C. A. Rosen, M. Ahmad, R. W. Alexander, and R. M. Medford.** 1993. Vascular cell adhesion molecule-1 (VCAM-1) gene transcription and expression are regulated through an antioxidant-sensitive mechanism in human vascular endothelial cells. J. Clin. Investig. **92:**1866–1874.
25. **Muller, W. A.** 2003. Leukocyte-endothelial-cell interaction in leukocyte transmigration and the inflammatory response. Trends Immunol. **24:**326–333.
26. **Rahman, A., J. Kefer, M. Bando, W. D. Niles, and A. B. Malik.** 1998. E-selectin expression in human endothelial cells by TNF-α-induced oxidant generation and NF-κB activation. Am. J. Physiol. (Lung Cell Mol. Physiol.) **275:**L-533–L-544.
27. **Springer, T. A.** 1995. Traffic signals on endothelium for lymphocyte recirculation and leukocyte emigration. Annu. Rev. Physiol. **57:**827–872.
28. **Touyz, R. M., F. Tabet, and E. L. Schiffrin.** 2003. Redox-dependent signalling by angiotensin II and vascular remodelling in hypertension. Clin. Exp. Pharmacol. Physiol. **30:**860–866.
29. **Volpp, B. D., W. M. Nauseef, J. E. Donelson, D. R. Moser, and R. A. Clark.** 1989. Cloning of the cDNA and functional expression of the 47-kilodalton cytosolic component of human neutrophil respiratory burst oxidase. Proc. Natl. Acad. Sci. USA **86:**7195–7199.
30. **Wajant, H., F. Henkler, and P. Scheurich.** 2001. The TNF-receptor-associated factor family. Scaffold molecules for cytokine receptors, kniases and their regulators. Cell. Signalling **13:**389–400.
31. **Xu, Y.-C., R. F. Wu, Y. Gu, Y. S. Yang, M.-C. Yang, F. E. Nwariaku, and L. S. Terada.** 2002. Involvement of TRAF4 in oxidative activation of c-Jun N-terminal kniase. J. Biol. Chem. **277:**28051–28057.